MITSUBISHI ELECTRIC RESEARCH LABORATORIES
https://www.merl.com

Extended Kalman Filter-based Predictive Maintenance of High-Voltage DC/DC Converter

Rahman, Syed; Liu, Dehong; Menner, Marcel; Wang, Yebin; Takegami, Tomoki

TR2023-131 October 18, 2023

Abstract

Isolated converters are the ideal candidate for high-gain DC/DC converter applications. Although the design of converters considers safety margins and derating requirements to ensure acceptable performance until the end of product life, it does not completely rule out any early component failure. It is inevitable that the post-deployment stresses result in component aging and subsequent failure before the end of its useful life. To minimize downtime, early failure signatures need to be detected for predictive maintenance, which requires continuous/periodic monitoring of critical components. This paper presents an Extended Kalman Filter (EKF)-based predictive maintenance algorithm of a 2kW, 270V/28V DC/DC converter. The detailed mathematical framework and observability analysis highlighting the feasibility of state/parameter estimation are presented. Based on observability analysis, the converter operating condition is devised such that accurate parameter estimation is achievable at a lower sensor sampling rate (equal to the switching time period). The significance of module-exclusive measurements on the observability and estimation of parameters is also discussed for a two-module system. The analyses presented are validated with detailed simulation results for single (2kW) and double (2x2kW) modules to estimate parameters of the filter inductor and the output capacitor.

IEEE Industrial Electronics Society (IECON) 2023

Mitsubishi Electric Research Laboratories, Inc.
201 Broadway, Cambridge, Massachusetts 02139

Extended Kalman Filter-based Predictive Maintenance of High-Voltage DC/DC Converter

Syed Rahman[1,2], Dehong Liu[1], Marcel Menner[1], Yebin Wang[1], and Tomoki Takegami[3]

[1]Mitsubishi Electric Research Laboratories (MERL), Cambridge, MA 02139, USA
[2]Dept. of Elec. & Comp. Engr., Texas A&M University, College Station, TX 77840, USA
[3]Advanced Technology R&D Center, Mitsubishi Electric Corporation, Hyogo, Japan
{rsyed,liudh,menner,yebinwang}@merl.com, Takegami.Tomoki@dy.MitsubishiElectric.co.jp

***Abstract*—Isolated converters are the ideal candidate for high-gain DC/DC converter applications. Although the design of converters considers safety margins and derating requirements to ensure acceptable performance until the end of product life, it does not completely rule out any early component failure. It is inevitable that the post-deployment stresses result in component aging and subsequent failure before the end of its useful life. To minimize downtime, early failure signatures need to be detected for predictive maintenance, which requires continuous/periodic monitoring of critical components. This paper presents an Extended Kalman Filter (EKF)-based predictive maintenance algorithm of a 2kW, 270V/28V DC/DC converter. The detailed mathematical framework and observability analysis highlighting the feasibility of state/parameter estimation are presented. Based on observability analysis, the converter operating condition is devised such that accurate parameter estimation is achievable at a lower sensor sampling rate (equal to the switching time period). The significance of module-exclusive measurements on the observability and estimation of parameters is also discussed for a two-module system. The analyses presented are validated with detailed simulation results for single (2kW) and double (2×2kW) modules to estimate parameters of the filter inductor and the output capacitor.**

***Index Terms*—Predictive maintenance, parameter estimation, extended Kalman filter, DC/DC converter, observability.**

I. Introduction

With the development of efficient wide-bandgap semiconductors and high-frequency magnetic components, the fast-switching power converter technology is quickly replacing the conventional low-frequency transformers [1]. This paradigm shift in power converter technology helps in achieving high power density, improved efficiency, and optimal control [2]. However, these efforts also reduce the footprints and consequently smaller surface areas to dissipate heat, resulting in complex thermal design and soft-switching requirements to achieve high reliability, especially in custom-built power systems such as aircraft. To ensure reliability, design features such as over-design, and redundancies are employed [3].

Post-deployment, the components are subjected to extreme operating conditions, mechanical shocks, and load transients. Continuous exposure to these conditions ages the component [4]. To ensure acceptable performance throughout the product life, the components are designed with safety margins, considering the derating requirements. However, this practice does not eliminate the chance of component failures. Capacitor and semiconductor failure account for 51% of power converters [5]. To address this concern, fault diagnosis algorithms are used. The fault diagnosis algorithms are a reactive approach and are either signal processing-based or model-based. In the first method, the diagnostic signal is searched for a fault signature to identify the fault, whereas model-based algorithms use analytical knowledge of the power converters, and employ diagnostic strategies such as sliding-mode observers, state estimation, etc. [4], [5].

To minimize unscheduled maintenance, health monitoring of components (to predict early failure) is proposed in the literature. The philosophy here is to observe the fault precursors of different components. For example, the effective series resistance (ESR) value is a good indicator of the capacitor's health [6]. These precursors may not be directly measurable and must be estimated. The estimation methods are either data-driven or model-based. Data-driven methods are mostly based on machine learning and require existing input data for hypothesis formulation and training [7]. On the other hand, the model-based methods include Kalman filters, sliding mode observer, and Luenberger observers. These methods are dependent on developing a reliable model of the power converter [8], including parasitic, as most precursors are parasitic in nature. The other important aspect is the selection of sensor measurements, which dictates the observability and estimation of state variables [9].

Extended Kalman Filter (EKF)-based techniques are used in DC/DC converters for implementing sensorless voltage control algorithm ([10]–[12]) and parameter-estimation based fault diagnostics in DC/DC converters [13]–[15]. Non-isolated DC/DC converters are considered for fault diagnosis.

This paper extends these efforts and implements the EKF-based parameter estimation for a full-bridge DC/DC converter. Detailed state-space modeling considering the component parasitics is presented. This model is then augmented using the Jacobian method (parameter drift estimation model) to include the dynamics and cross-coupling of parameters and the original states. As output voltage and current are sensed conventionally for closed-loop control in DC/DC converters,

This work was finished when Syed Rahman was an intern at MERL.

these measured signals are used in the EKF. Observability for the joint state and parameter estimation is determined by linearizing at all operating points (consisting of both transient and steady-state). The modeling and analysis help in concluding that capacitance value is not observable during steady state, and requires transient states for estimation. This background is then used for devising a control-side based duty-cycle induced transients, which improves the capacitance value estimation, and also helps in reducing the sensor sampling time requirement. These analyses are extended to two parallelly connected DC/DC converter modules, measuring the modular inductor current and the common output voltage. The issue of loss of observability of output-side capacitance values is also highlighted and validated through simulation results.

The remainder of this paper is structured as follows. Section II briefly discusses the DC/DC converter under study, including the topology in Section II-A, parameter design in Section II-B, and fundamentals of dynamic system modeling and augmented matrix construction for the power converter in Section II-C. Observability of the state variables and component parameters of the power converter is discussed in Section III-A. This concept is extended to two parallelly connected modules in Section III-B. The detailed simulation results captured to validate the analysis are discussed in Section IV. Finally, Section V concludes the paper.

II. System Under Study

A. Topology

The isolated DC/DC converter topology is shown in Fig. 1. It consists of a MOSFET-based H-bridge on the input side, and a full-bridge diode rectifier at the output side, isolated by a high-frequency transformer. With MOSFETs on the input side, this converter is controlled by modulating the duty cycle of the primary side switches to generate a square or quasi-square voltage at the transformer input. The secondary side diodes conducts to transfer power to the output.

For efficient predictive maintenance, the parasitics of the circuit are also considered. Parasitics include forward resistance of primary MOSFETs (R_{mp}), voltage drop across diode (V_d), inductor internal resistance (R_{lk}) and effective series resistance (ESR) of the capacitor (R_c). The converter is modeled assuming continuous conduction mode operation.

B. Parameter Design

This converter is designed to step down 270V DC to 28V DC. The power converter is rated for 2kW. Assuming rated efficiency of 95%, the rated input current is 8A, whereas the output current is 71A. The duty cycle (d) of the converter is given by

$$d = \frac{V_o}{n(V_{in} - 2V_M) - 2V_d - R_{lk}I_L}, \tag{1}$$

where V_M is the voltage drop across the MOSFET, and V_d is the drop across the secondary diodes. For an operational duty cycle of 0.7, the transformer turns ratio is obtained to be 1/6.5.

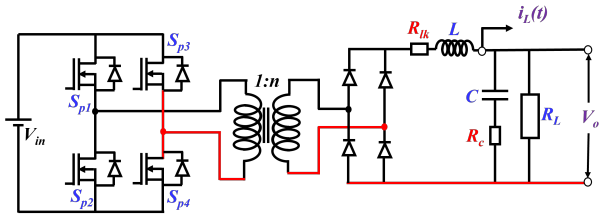

Fig. 1. Full-Bridge DC/DC Converter.

Assuming a current ripple of 10% of the rated output current (71A), the filter inductor (L_f) is given by [16]

$$L_f = \left(\frac{n(V_{in} - 2V_M) - 2V_d - V_o}{f\Delta I_{L_{max}}}\right) d. \tag{2}$$

The capacitor (C_f) for a voltage ripple of 3% is given by [16]

$$C_f = \left(\frac{\Delta I_{L_{max}}}{f\Delta V_{o_{min}}}\right) d. \tag{3}$$

This gives a filter inductor of 14.5 µH, and filter capacitor of 0.11mF. Considering safety margin of 50% for the inductor, it is taken as 22µH/100A, whereas the capacitor is rated for 220µF. The capacitors are realized through parallel combination of Al electrolytic capacitors (PCH1H181MCL1GS - 82µF/50V) and ceramic capacitors (KCM55QR71J106KH01K - 10µF/63V). The primary side MOSFET is rated for 1000V/32A (C3M0065100K). The secondary side diodes are rated for 100V/100A (VS-100BGQ100).

C. Converter Modeling

The DC/DC converter modeling, considering the two operating modes, is given by

$$\begin{bmatrix}\dot{i}_L \\ \dot{v}_c\end{bmatrix} = \begin{bmatrix}-\frac{R_{eq}}{L} & \frac{-G_a}{L} \\ \frac{G_a}{C} & \frac{-G_a}{R_L C}\end{bmatrix}\begin{bmatrix}i_L \\ v_c\end{bmatrix} + \begin{bmatrix}u_1 \\ 0\end{bmatrix}, \tag{4}$$

$$y = \begin{bmatrix}R_c G_a & G_a \\ 1 & 0\end{bmatrix}\begin{bmatrix}i_L \\ v_c\end{bmatrix}, \tag{5}$$

where $R_{eq} = R_{lk} + R_c G_a + 2ndR_{mp}$, $y = [V_o, i_L]^\top$, $G_a = 1/(1+r_a)$, $r_a = R_c/R_L$, $u_1 = V'_{in}/L$, and $V'_{in} = ndV_{in} - 2V_d$. A similar analysis can be carried out for the discontinuous conduction mode, by considering the zero inductor current period in addition to the two operating modes.

As discussed in Section II-A, this model contains the parasitic element of each component. These parasitics are the most important failure precursors. For example, in case of Al electrolytic capacitor, the deteriorating health is reflected in terms of its reduced capacitance and increased ESR value. In case of inductor, thermal aging results in increased core-losses and self-heating. This continuous self-heating deteriorates the winding insulation, finally resulting in an inter-turn fault of the inductor (reflected as a reduced inductance). Similarly, increasing ON-state resistance is a strong failure precursor for MOSFETs [17]. With the current state-space model, it is observed that the health status of the converter, owing to

aging or ambient temperature variation, can be characterized by $[L, C, R_c]$. It is arguably true that compared with variables i_L and v_c, the quantities $[L, C, R_c]$ are slowly time-varying and can be treated as parameters, *i.e.*, $\dot{L} = 0, \dot{C} = 0, \dot{R}_c = 0$. For estimation of the parameters, the augmented matrix consisting of cross-coupling/inter-connection terms between these parameters and the actual state variables is exploited.

The augmented converter model is given by

$$\begin{bmatrix} \dot{i}_L \\ \dot{v}_c \\ \dot{L} \\ \dot{C} \\ \dot{R}_c \end{bmatrix} = \begin{bmatrix} -\frac{R_{eq}}{L} & \frac{-G_a}{L} & a_{13} & 0 & a_{15} \\ \frac{G_a}{C} & \frac{-G_a}{R_L C} & 0 & a_{24} & a_{25} \\ 0 & 0 & 0 & 0 & 0 \\ 0 & 0 & 0 & 0 & 0 \\ 0 & 0 & 0 & 0 & 0 \end{bmatrix} \begin{bmatrix} i_L \\ v_c \\ L \\ C \\ R_c \end{bmatrix} + \begin{bmatrix} u_1 \\ 0 \\ 0 \\ 0 \\ 0 \end{bmatrix}, \tag{6}$$

$$y = \begin{bmatrix} R_c G_a & G_a & 0 & 0 & -\frac{G_a^2}{R_L} V_D \\ 1 & 0 & 0 & 0 & 0 \end{bmatrix} \begin{bmatrix} i_L \\ v_c \\ L \\ C \\ R_c \end{bmatrix}, \tag{7}$$

where $a_{13} = (R_{eq} I_L + G_a V_c)/L^2$, $a_{15} = \frac{Ga^2}{L R_L} V_D$, $a_{24} = \frac{Ga}{R_L C^2} V_D$, and $a_{25} = \frac{G_a^2}{C R_L^2} V_D$, and $V_D = V_c - R_L I_L$. In (6), I_L and V_c correspond to the inductor current and capacitor voltage at the operating point of the converter.

To avoid numerical discrepancies, this model can be expressed using the state vector X = $[i_L, v_c, \theta_1, \theta_2, R_c]^\top$ as state variables, where $\theta_1 = 1/L$ and $\theta_2 = 1/C$. With these state variables, the augmented converter model admits the following state space representation:

$$\dot{X} = \underbrace{\begin{bmatrix} -R_{eq}\theta_1 & -G_a\theta_1 & \theta_{13} & 0 & \theta_{15} \\ G_a\theta_2 & \frac{-G_a\theta_2}{R_L} & 0 & \theta_{24} & \theta_{25} \\ 0 & 0 & 0 & 0 & 0 \\ 0 & 0 & 0 & 0 & 0 \\ 0 & 0 & 0 & 0 & 0 \end{bmatrix}}_{A_x} X + \underbrace{\begin{bmatrix} \theta_1 \\ 0 \\ 0 \\ 0 \\ 0 \end{bmatrix}}_{B_u} V'_{in}, \tag{8}$$

$$y = \underbrace{\begin{bmatrix} R_c G_a & G_a & 0 & 0 & -\frac{G_a^2}{R_L} V_D \\ 1 & 0 & 0 & 0 & 0 \end{bmatrix}}_{C_x} X, \tag{9}$$

where $\theta_{13} = -R_{eq} I_L - G_a V_c$, $\theta_{15} = \frac{G_a^2 \theta_1}{R_L} V_D$, $\theta_{24} = -\frac{Ga}{R_L} V_D$, and $\theta_{25} = \frac{G_a^2}{R_L^2} V_D$.

III. Observability Analysis

A. Single DC/DC Converter

The objective here is to analyze the observability of the state variables, which is dependent upon the number of measurements, and linearization point. For further analysis, the state model is discretized for sampling period T_s, and is given by

$$X_k = A_d X_{k-1} + B_\theta u_k, \tag{10}$$

where $A_d = I + T_s A_x$, $B_\theta = T_s B_u$, $u_k = V'_{in}$, and A_x and B_u are obtained from (8).

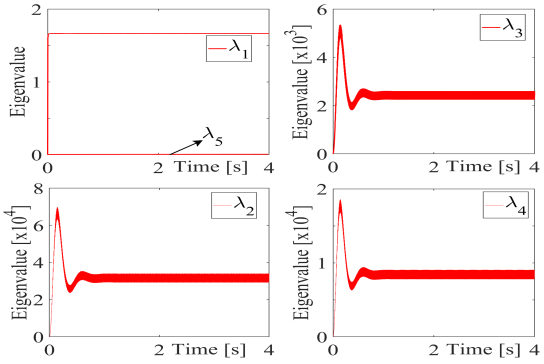

Fig. 2. Eigenvalues plots of the system with five state variables.

The next step is to construct the observability matrix ($\mathcal{O}$)

$$\mathcal{O} = \begin{bmatrix} C_x & C_x A_d & . & . & C_x A_d^{n-1} \end{bmatrix}^\top, \tag{11}$$

where n is the number of state variables.

The last step is to find out the eigenvalues of the observability matrix given by $|\mathcal{O} - \lambda I| = 0$. The eigenvalues obtained for the system depend upon the point of linearization. As observed in (8) and (9), the term $(V_c - R_L I_L)$ tends to almost zero once the converter reaches a steady state.

To address this, the process of eigenvalue estimation is carried out at all time steps (instead of one linearization point), including transient and steady-state periods. This requires the inductor current (I_L) and capacitor voltage (V_c) to be estimated beforehand. To address this, the power converter is simulated in MATLAB Simulink. The converter response for a time period of 4ms with a sampling time of 10ns is recorded in terms of I_L and V_c. These values are then used for the estimation of eigenvalues at each of the operating points. The eigenvalues plot is shown in Fig. 2. From the plot, it can be inferred that only four eigenvalues are observable, whereas the fifth eigenvalue remains close to zero, *i.e.*, with a maximum value of 10^{-12} and a minimum of 0. To exactly determine the observable states, the above process is repeated considering a new state vector $X^{(1)} = [i_L, v_c, \theta_1, \theta_2]^\top$ (without R_c). The eigenvalue plot for the system is shown in Fig. 3, which confirms their observability during the transient state. Conclusively, through the observability analysis, the four observable states (during both steady-state and transients) are selected, which helps in the construction of the state vector $X^{(1)}$.

Post observability analysis, the next step is to estimate the state vector using the EKF-based estimation. There are two main steps in EKF, *i.e.*, state predict and state update. The state equation (10) is used for the state variable prediction ($\hat{x}_k^-$), whereas the covariance matrix (P_k^-) is predicted using [18]

$$P_k^- = A_d P_{k-1} A_d^\top + Q, \tag{12}$$

where Q is the process noise covariance matrix, and P_{k-1} is the covariance matrix at previous sample. Post measurements (z_k), the state variable estimate ($\hat{x}_k$) and the process covariance matrix (P) are updated using [18]

$$\hat{x}_k = \hat{x}_k^- + K_k(z_k - y), \tag{13}$$

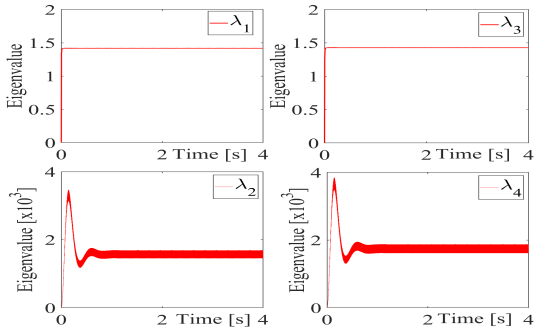

Fig. 3. Eigenvalue plots of the system with four state variables.

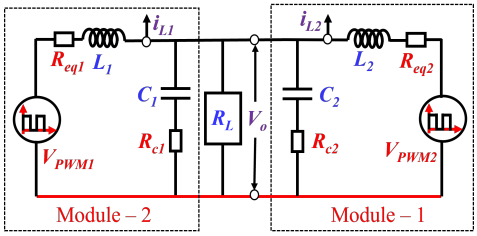

Fig. 4. Equivalent circuit of two converter modules connected in parallel.

$$P_k = P_k^- - K_k C_x P_k^-, \tag{14}$$

where $K_k = P_k^- C_x^\top (C_x P_k^- C_x^\top + R)^{-1}$ is the Kalman filter gain, and R is the measurement noise covariance matrix. The initialization used and estimation performance of the EKF is detailed in Section IV-A.

B. Double Parallelly Connected DC/DC Converter Modules

In the case of two parallel modules controlled with average control (i.e., the same duty cycle applied to both converters), the output-side capacitors are fastly deteriorated by the circulating currents. The modeling of this system is complex compared to the single module. The two parallelly connected converter modules, as shown in Fig. 4, are now analyzed for observability. V_{PWM1} and V_{PWM2} are the voltages at the output of the secondary-side diode rectifier in the module. In this setting, the state vector is defined as $X^{(2)} = [i_{L1}, i_{L2}, v_{c1}, v_{c2}]^\top$, with two inputs ($[V_{in1}, V_{in2}]^\top$), and three measurements ($y = [V_o, i_{L1}, i_{L2}]^\top$). The dynamic relations for the parallelly connected modules are given by

$$\underbrace{\begin{bmatrix} L_1 & 0 & R_{c1}C_1 & 0 \\ 0 & L_2 & 0 & R_{c2}C_2 \\ 0 & 0 & C_1 & C_2(1+\frac{R_{c2}}{R_L}) \\ 0 & 0 & -R_{c1}C_1 & R_{c2}C_2 \end{bmatrix}}_{A_1} \dot{X}$$
$$= \underbrace{\begin{bmatrix} -R_{eq1} & 0 & -1 & 0 \\ 0 & -R_{eq2} & 0 & -1 \\ 1 & 1 & 0 & \frac{-1}{RL} \\ 0 & 0 & 1 & -1 \end{bmatrix}}_{A_2} X + \underbrace{\begin{bmatrix} u_a \\ u_b \\ 0 \\ 0 \end{bmatrix}}_{B} \tag{15}$$

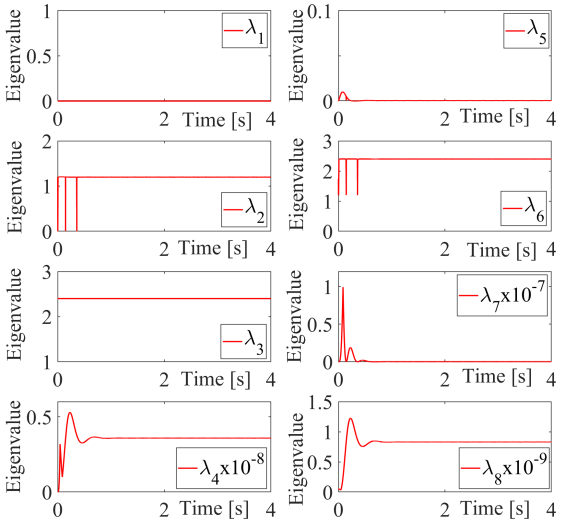

Fig. 5. Eigenvalue plot for the state vector.

Upon simplification, the state equation is obtained as

$$\dot{X} = A_1^{-1} A_2 X + A_1^{-1} B \tag{16}$$

The output equation is given by

$$y = \begin{bmatrix} z/\theta & z/\theta & \frac{R_L R_{c2}}{\theta} & 1 - \frac{R_{c2}}{\theta}(R_{c1}+R_L) \\ 1 & 0 & 0 & 0 \\ 0 & 1 & 0 & 0 \end{bmatrix} X, \tag{17}$$

where $z = R_{c1}R_{c2}R_L$, $\theta = R_{c1}R_{c2} + R_{c2}R_L + R_L R_{c1}$, $R_{eq1} = 2n_1 d_1 R_{mp1} + R_{lk1}$, $R_{eq2} = 2n_2 d_2 R_{mp2} + R_{lk2}$, $u_a = n_1 d_1 V_{in1} - 2V_{d1}$, and $u_b = n_2 d_2 V_{in2} - 2V_{d2}$. For the modules, d, n, V_d, and V_{in} represent the duty cycle, transformer ratio, diode voltage drop, and input voltage respectively.

Using (16), the augmented converter model is constructed considering the additional parameters of the two modules. The state vector for the augmented model is given by $X^{(3)} = [i_{L1}, i_{L2}, v_{c1}, v_{c2}, L_1, L_2, C_1, C_2]^\top$. The entire process of discretization and estimation of eigenvalues (discussed in III-A) is repeated. For this exercise, the L and C values in the second module are assumed to be different *i.e.*, $L_2 = 1.05L_1$, $R_{lk2} = 0.85R_{lk1}$, $C_2 = 1.1C_1$, and $R_{c2} = 1.2R_{c1}$. Using these values, the two-parallel modules are simulated in MATLAB/Simulink to get inductor currents, and voltage capacitors during transient state of 4ms. The eigenvalue plot is shown in Fig. 5. It can be observed here that the two eigenvalues are unobservable, whereas the other six variables are observable. This suggests that the exclusive inductor current measurements are vital in $[L_1, L_2]$ estimation. On the other hand, the output voltage measurement, which corresponds to the cumulative effect of the capacitors, is not sufficient for $[C_1, C_2]$ estimation.

Similar to the single-module analysis, the EKF is implemented using the augmented converter model and (17). The validation of these findings and the EKF tracking performance is detailed in Section IV-C.

IV. Simulation Results

For validation of the analyses, a MATLAB/SIMULINK-based simulation model is developed. The parameter specification of the DC/DC converter module are detailed in Table I. In this SIMSCAPE model, the DC/DC converter is simulated to generate the measurements (z_k) along with the input signals. These inputs and measurements are passed on to the EKF to estimate the parameters. The EKF is implemented in the SIMSCAPE model using the "MATLAB function" block.

For this simulation, it is assumed that the current and voltage sensors are 99% accurate of the rated values and the measurement reading is 1% error of the rated values *i.e.*, $R = \text{diag}\{0.71^2, 0.28^2\}$. The initial values are $x_{0|0} = [0, 0, 3.03 \times 10^4, 1.818 \times 10^4]^\top$ and $P_{0|0} = Q$.

A. EKF Performance for single-module of DC/DC Converter

As discussed in Section III, the coefficient $\frac{\partial v_c}{\partial C} = -\frac{G_a}{R_L}(V_c - R_L I_L)$ tends to zero during the steady state, making C unobservable, and it can only be observed during the transient state. For this estimation, a train of control-induced duty-cycle change is applied by continuously with d varying between 0.5 to 0.7 for every 2ms. As power transfer is controlled for duty modulation of the input-side converter, the varying duty cycle is used for pulse generation of the primary-side H-Bridge. For these transient pulses, the simulation results obtained are shown in Fig. 6. As observed, the EKF-estimated inductor current ($i_{L_{est}}$) and capacitor voltage ($v_{c_{est}}$) are in close approximation to the measured signals ($i_{L_{meas}}, v_{c_{meas}}$). This high accuracy of estimation is achieved as a combination of the state-space model and signal measurements (V_o and i_L).

The parameter estimation shows that the EKF is capable of estimating the true L and C values, after the initial converter starting transients. Secondly, as the duty-cycle change is producing transient behavior, the EKF estimation uses an average model (duty-cycle read as a numerical value), and the sampling frequency of the sensors and the step size of the EKF is equal to that of the converter switching frequency (80kHz). This method of estimation can be used for periodic monitoring, before actual operation. If applied during normal operation, the output voltage variations will exceed the allowable limits.

B. Real-time estimation of Filter Inductance (L)

Inductors are not a major contributor to the overall faults in power converters. However, for high-current applications, the dissipation losses in the indicator tends to increase for higher temperatures. Continuous operation impacts the magnetic wire insulation culminating into an inter-turn fault. These faults generally occur during the real-time operation. Thus, to predict these fault, L must be estimated in real-time. For this real-time estimation, the previously designed duty-cycle based method is unacceptable, as it results in unacceptable output voltage variation. For this estimation, the duty-cycle induced switching transients are utilized by sensing the duty cycle from the control board. For this purpose, for 80kHz switching frequency, the sensor sampling rate of 0.25µs is used, *i.e.*, 50 samples in each switching cycle. The simulation results

TABLE I
Parameter specification of Single DC/DC Converter

Parameter	Specification	Parameter	Specification
Output Voltage	28 V	Input Voltage	270 V
Rated Power	2.00 kW	Inductor Current	71 A
Transformer ratio	1:6.5	Filter inductor	22 µH
Filter capacitor	0.22 mF	Capacitor ESR	0.94 mΩ
Primary MOSFET	65 mΩ	Diode drop	0.82 V
Inductor resistance	5 mΩ	Duty cycle	0.7

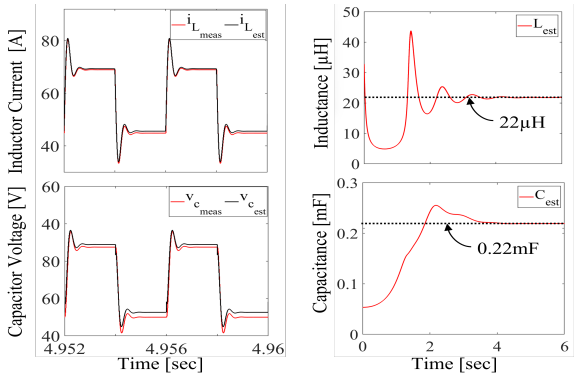

(a) (b)

Fig. 6. (a) Tracking performance of the state variables i_L and v_c. (b) Estimation of L and C for a single module.

obtained are shown in Fig. 7. It can be observed here that the EKF is now capable of estimating the switching ripple in the inductor current and L value. When the inductance value is decreased at t = 0.6s (emulating an inter-turn fault), the inductor current's peak-to-peak ripple changes. This updated information is passed to EKF through measurements. This transition invoke the EKF to estimate the new values of the state vector including the inductor value.

C. EKF Performance for multiple DC/DC Converter modules

For validation of the analysis presented in Section III-B, two parallelly connected DC/DC converter modules are simulated. These two converters are operated with the same duty cycle signal, and the duty cycle is continuously varied between 0.5 to 0.7 for every 2ms. The simulation result is shown in Fig. 8. It can be observed here that initially the EKF tracks L_1, L_2, C_1, C_2 perfectly. However, once the capacitance value of the second module is changed from 0.24mF to 0.18mF, the algorithm reflects this change by equaling both capacitance values (to 2mF) and their sum equal to the total capacitance (4mF). This occurs due to the measurement of common output voltage, which is truly a reflection of the two module output voltages. Any capacitance change will be reflected as an average effect of the two converters on the output voltage. This observation is in line with the reduced rank of eigenvalues, suggesting loss of observability of two signals, *i.e.*, C_1 and C_2 (discussed in Section (III-B). On the other hand, the capacitance change has little impact on the inductances' tracking, which remains fairly constant. This

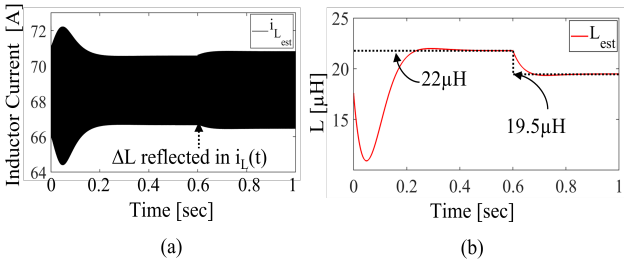

Fig. 7. (a) Change in inductor current ripple due to inductor change at 0.6s, (b) Response of EKF based real-time filter inductance estimation.

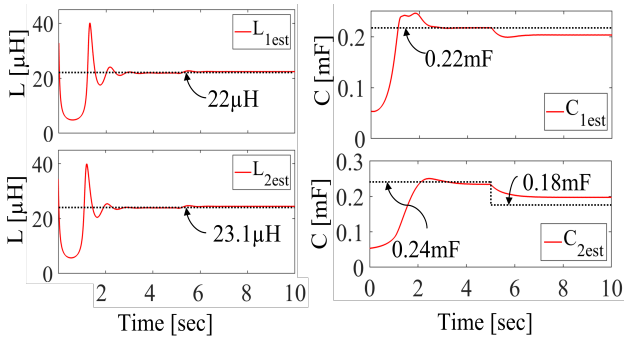

Fig. 8. EKF tracking performance for two modules validating the inability to accurately estimate the capacitance values post disturbance.

validates the fact that L_1 and L_2 are distinctly observable in the double module configuration.

V. Conclusion

This paper explored the EKF-based parameter estimation of full bridge DC/DC converter for single and multiple modules. In single module analysis, it is observed that all the parasitic resistances are lumped together in the state matrix, thereby making it difficult to estimate them as state variables individually. Using observability analysis, the unobservable states are identified and segregated to form a state vector consisting of observable states. For the state vector $[i_l, v_c, L, C]^\top$, it is observed that applying the control-side induced duty-cycle transients helps in accurate estimation of L and C (during the transient period). This method also shows that parameters can be estimated using the average value of the duty cycle, with the sensor sampling rate equal to the switching time period. However, for real-time estimation, as no control-side transients can be induced (to meet the operating voltage allowable range), the sampling rate must be increased to reflect the variation of the steady-state duty cycle signal (instead of an average value). On the other hand, for two modules, it is observed that using the common output voltage signal results in loss of observability of output side capacitors. For any perturbation in these capacitors, the algorithm fails to distinctly identify the source of change. This suggests that using individual capacitor voltage as measurements will result in a higher rank and better observability.

References

[1] T. Ilahi, T. Izhar, S. M. Qaisar, U. T. Shami, M. Zahid, A. Waqar, and A. Alzahrani, "Design and performance analysis of ultra-wide bandgap power devices-based EV fast charger using bi-directional power converters," *IEEE Access*, vol. 11, pp. 25 285–25 297, 2023.

[2] J. E. Huber and J. W. Kolar, "Volume/weight/cost comparison of a 1MVA 10kV/400V solid-state against a conventional low-frequency distribution transformer," in *2014 IEEE Energy Conversion Congress and Exposition (ECCE)*. IEEE, 2014, pp. 4545–4552.

[3] N. Swaminathan and Y. Cao, "An overview of high-conversion high-voltage DC–DC converters for electrified aviation power distribution system," *IEEE Transactions on Transportation Electrification*, vol. 6, no. 4, pp. 1740–1754, 2020.

[4] S. S. Khan and H. Wen, "A comprehensive review of fault diagnosis and tolerant control in DC-DC converters for DC microgrids," *IEEE Access*, vol. 9, pp. 80 100–80 127, 2021.

[5] G. K. Kumar and D. Elangovan, "Review on fault-diagnosis and fault-tolerance for DC–DC converters," *IET Power Electronics*, vol. 13, no. 1, pp. 1–13, 2020.

[6] Z. Zhao, P. Davari, W. Lu, H. Wang, and F. Blaabjerg, "An overview of condition monitoring techniques for capacitors in DC-link applications," *IEEE Transactions on Power Electronics*, vol. 36, no. 4, pp. 3692–3716, 2020.

[7] S. Zhao and H. Wang, "Enabling data-driven condition monitoring of power electronic systems with artificial intelligence: Concepts, tools, and developments," *IEEE Power Electronics Magazine*, vol. 8, no. 1, pp. 18–27, 2021.

[8] J. Poon, P. Jain, I. C. Konstantakopoulos, C. Spanos, S. K. Panda, and S. R. Sanders, "Model-based fault detection and identification for switching power converters," *IEEE Transactions on Power Electronics*, vol. 32, no. 2, pp. 1419–1430, 2016.

[9] Y. Wang, H. Fang, L. Zhou, and T. Wada, "Revisiting the state-of-charge estimation for lithium-ion batteries: A methodical investigation of the extended Kalman filter approach," *IEEE Control Systems Magazine*, vol. 37, no. 4, pp. 73–96, 2017.

[10] M. Y. Candan and M. M. Ankarali, "Extended Kalman filter based state and parameter estimation method for a buck converter operating in a wide load range," in *2020 IEEE Energy Conversion Congress and Exposition (ECCE)*. IEEE, 2020, pp. 3238–3244.

[11] W. Zhifu, W. Yupu, and R. Yinan, "Design of closed-loop control system for a bidirectional full bridge DC/DC converter," *Applied Energy*, vol. 194, pp. 617–625, 2017.

[12] M. Y. Candan and M. M. Ankarali, "Steady-state hybrid extended Kalman filter based sensorless voltage controller for a phase-shifted full-bridge converter," *IET Power Electronics*, vol. 16, no. 1, pp. 53–63, 2023.

[13] M. Ahmeid, M. Armstrong, S. Gadoue, M. Al-Greer, and P. Missailidis, "Real-time parameter estimation of DC–DC converters using a self-tuned Kalman filter," *IEEE Transactions on Power Electronics*, vol. 32, no. 7, pp. 5666–5674, 2016.

[14] A. Izadian and P. Khayyer, "Application of Kalman filters in model-based fault diagnosis of a DC-DC boost converter," in *IECON 2010-36th Annual Conference on IEEE Industrial Electronics Society*. IEEE, 2010, pp. 369–372.

[15] E. Ribeiro, A. M. Cardoso, and C. Boccaletti, "Fault diagnosis in unidirectional non-isolated dc-dc converters," in *2014 IEEE Energy Conversion Congress and Exposition (ECCE)*. IEEE, 2014, pp. 1140–1145.

[16] C. Andersson, "Design of a 2.5 kw DC/DC fullbridge converter," 2011.

[17] H. Givi, E. Farjah, and T. Ghanbari, "A comprehensive monitoring system for online fault diagnosis and aging detection of non-isolated DC–DC converters' components," *IEEE Transactions on Power Electronics*, vol. 34, no. 7, pp. 6858–6875, 2018.

[18] A. Pereira, C. Duarte, and W. Gora, "Performance improvement of a buck converter using Kalman filter," *Master thesis*, 2015.